Journal of Power Sources 217 (2012) 530–537

Contents lists available at SciVerse ScienceDirect

Journal of Power Sources

journal homepage: www.elsevier.com/locate/jpowsour

Correlationship between electrode mechanics and long-term cycling performance for graphite anode in lithium ion cells

Honghe Zheng [a,b,*], Li Zhang [a], Gao Liu [b], Xiangyun Song [b], Vincent S. Battaglia [b]

[a] School of Energy, Soochow University, Suzhou, Jiangsu 215006, PR China
[b] Lawrence Berkeley National Laboratory, 1 Cyclotron Rd, Berkeley, CA 94720, USA

HIGHLIGHTS

- Cycling performance of a graphite anode is correlated with its mechanics.
- The graphite laminate of lower modulus has longer durability.
- Impedance rise is responsible for the electrochemical deterioration.
- Crack formation and propagation within the laminate causes the impedance rise.

ARTICLE INFO

Article history:
Received 2 April 2012
Received in revised form
8 June 2012
Accepted 9 June 2012
Available online 26 June 2012

Keywords:
Lithium ion batteries
Graphite anode
Mechanical properties
Cycle life

ABSTRACT

In the development of lithium ion batteries for electric vehicle applications, much effort has been made in fabrication and optimization of active materials. Mechanical properties of the electrode laminate, which are also very critical determining the durability of the cell, have long been ignored. In this study, graphite laminates of the same chemical composition are prepared by using different mixing technologies. With similar breaking strength, Young's modulus of the laminate is found to be very different according to the mixing order. Electrochemical performances of the graphite laminates are investigated against Li anode and $Li[Ni_{1/3}Co_{1/3}Mn_{1/3}]O_2$ cathode, respectively. Long-term cycling performance is closely related with the Young's modulus of the graphite laminate. Whereas the laminates of low modulus cycles well during the investigated 600 deep charge–discharge cycles, the electrodes of high modulus fail at around 350 cycles. Electrochemical degradation mechanism for the laminate of high modulus is associated with the significant impedance rise aroused from mechanical failure. After the long-term cycling test, lots of cracks are observed on the high modulus electrode along the particle boundaries while the mechanical integrity of the low modulus laminate is well maintained.

1. Introduction

Long-term cycling capability (3000–5000 deep charge–discharge cycles) with 10–15 year calendar life is one of the important requirements for lithium ion batteries for electric vehicle (EV) and plug-in hybrid electric vehicle (PHEV) applications. To attain this goal, much effort has been made in fabricating and optimizing active materials as active materials are always believed to be the key determining the overall electrochemical performances of Li-ion batteries. However, this is far from enough. Mechanics and microstructure of the composite electrode laminate are also very important in determining the performance and durability of the cell, especially for large format batteries for transportation applications [1–3]. In view of this, a comprehensive understanding of the design of high quality electrodes is very essential to improve the overall electrochemical performances of Li-ion batteries. However, to the best of our knowledge, less attention has been paid to this study.

Many lithium-storage materials are known undergoing a certain extent of volume change (expansion/contraction) during electrochemical processes as a result of Li insertion and extraction. Several groups have modeled the internal stresses within active material particles generated by volume change during charge–discharge cycles [4–7]. It is assumed that the internal stress is able to bring about the breakage of active material particles and thus lead to a significant capacity loss of the cell. Several models have been developed to interpret the mechanical and micro-structural

* Corresponding author. School of Energy, Soochow University, Suzhou, Jiangsu 215006, PR China. Tel.: +86 (0)512 65240544; fax: +86 (0)512 67870289.
E-mail addresses: hhzheng66@yahoo.com.cn, hzheng66@hotmail.com (H. Zheng).

0378-7753/$ – see front matter © 2012 Elsevier B.V. All rights reserved.
http://dx.doi.org/10.1016/j.jpowsour.2012.06.045

changes of different active materials. However, up to today, few direct and convincing evidences have been obtained to support this assumption, even after long-term deep charge–discharge cycles.

As the matter of fact, Li-ion battery electrode is a composite of active material, polymeric binder and carbon conductive additive, which has very complex microstructures. Mechanics of the electrode laminate are important physical properties evaluating the cooperation between the electrode components. Not only the failure or degradation of any one electrode component reduces the electrochemical activity of the electrode, mechanical failure of the composite laminate also leads to severe electrochemical deterioration. Theoretically, mechanical failure of an electrode occurs preferentially at the weakest region of the laminate during electrochemical cycles. In this sense, it is less probable for the breakage of active material particles due to the strong chemical bond interaction. By contrast, there are only weak physical interactions at the phase interfaces between the electrode components. Therefore, crack of the electrode laminate should be more likely to occur along the phase boundaries. As the result, the physical and electrical connection between active particles is destroyed. A large resistance rise aroused from the electrical disconnection between the active particles can be a reason leading to electrochemical decline of the electrode. Understanding how the mechanical properties affect the electrode performances can help us reduce factors detrimental to battery performance and architect electrodes in a desired way. However, the influence of mechanical properties on the electrochemical performance for an electrode has not been taken into consideration in modeling electrode failure modes and predicting battery life [8,9].

Among different kinds of lithium-storage materials used in commercial lithium ion batteries, graphite are known having relatively large volume change ratio during lithiation compared with $Li_4Ti_5O_{12}$ anode material and many cathode materials such as $LiMn_2O_4$, $LiCoO_2$, $LiNi_{1/3}Co_{1/3}Mn_{1/3}O_2$, and $LiFePO_4$, etc. A volume expansion ratio of around 10% was reported for fully lithiated graphite particles [10,11]. To investigate the mechanical effects on the electrochemical performances of a graphite electrode, the composite laminates of the same chemical composition but different mechanical properties were prepared by using different mixing technologies of the slurries. A correlation between Young's modulus and long-term cycling performance of the graphite anode was developed. The underlying mechanisms in the correlation were discussed.

2. Experimental

A CGP-G8 graphite (from Conoco Phillips) was used as the anode material. Battery-grade acetylene black (AB) with an average particle size of 40 nm was acquired from Denka Singapore Private Ltd. Polyvinylidene difluoride (PVDF, KF1100) binder was supplied by Kureha, Japan. N-methylpyrrolidone (NMP) was purchased from Aldrich chemical company.

The slurries containing 88.8% graphite, 8% PVdF, and 3.2% acetylene black in NMP solvent were prepared. In preparation of the slurries, two different mixing sequences of the components were adopted. One sequence is to prepare a homogenous AB/PVDF/NMP mixture at first. The mixture was made by dissolving 10 g PVDF into 86 g anhydrous NMP. 4 g AB was then dispersed in the PVDF polymer solution. To thoroughly mix AB nanoparticles into the polymer solution, Branson 450 sonicator equipped with a solid horn was used. The sonic dispersion took 30 min till a very uniform mixture was formed. Slurry (I) was made by adding a targeted amount of CGP-G8 graphite into a certain amount of the premixed AB/PVDF/NMP mixture. The slurry was homogenized again by using a Polytron PT10-3S homogenizer at 4000 rpm for 15 min until viscous and uniform slurry was obtained. The other one mixing sequence is to mix the graphite material and acetylene black together in NMP solvent. The graphite/AB/NMP mixture was homogenized with Polytron PT10-3S homogenizer at a rate of 4000 rpm for 15 min. Slurry (II) was prepared by adding a calculated amount of PVDF into the premixed graphite/AB/NMP mixture. The slurry was further homogenized at a rate of 4000 rpm for 15 min. Five different slurries were obtained by mixing slurry (I) with slurry (II) at different ratios of 1:0, 2:1, 1:1, 1:2, and 0:1, respectively. All the slurries were subject to 5 more min homogenization before use.

Rheological properties of the slurry were measured by using Bohlin Gemini rheometer with a 60 mm diameter cone-and-plate measuring system, with the cone angle 2° and gap of truncated cone tip 56 μm. A stress-controlled mode was adopted in the determination in which the stress range was controlled from 1 to 300 Pa. All the samples were equilibrated at 25 °C for 15 min before test in order to remove any previous shear histories and to ensure that the constituent materials establish their equilibrium structures.

Electrode laminates were prepared by casting the slurries onto copper foil by doctor blade method. Through varying the height of the blade, all the electrode films were cast to have approximately the same loading of active material (around 6.5 mg cm^{-2}). Five different graphite laminates prepared with slurries containing slurry (I) and slurry (II) at 1:0, 2:1, 1:1, 1:2, and 0:1 ratios were referred to as laminate A, B, C, D, and E, respectively. All the electrode laminates were dried at 130 °C for 10 h under vacuum before use.

2.5 × 6 cm sections were cut out from the dried electrode laminate. In order to determine the electronic conductivity and mechanical properties of the electrode laminate, the electrode film was peeled off from the Cu substrate. The dc conductivity measurement was performed by using a Jandel equal-distance linear four-point probe apparatus with a Solartron 1286 Electrochemical Interface and a CorrWare software package. Breaking stress and Young's modulus of the electrode laminates were measured by using Chatillon TCD225 force measurement system. A stretching speed of 0.00125 mm s^{-1} was applied in this study. Determination for each sample was repeated 5 times.

Breaking stress is defined as the quotient of the maximum force applied onto the film till it breaks and the section area of the laminate. It is calculated from the following equation:

$$\text{Breaking stress} = (\text{maximum force})/(\text{width} \times \text{thickness}) \quad (1)$$

Strain is defined as the ratio of change in length versus the initial length of the laminate:

$$\text{Strain} = \text{length change}/\text{initial length} \quad (2)$$

Young's modulus is the ratio of stress with reference to the strain:

$$\text{Young' modulus} = \text{stress}/\text{strain} \quad (3)$$

Porosity of the electrode was calculated by taking into account of the true density of the mix obtained from X-ray measurements as described in our previous work [12]. The true density of graphite was obtained to be 2.1 g cm^{-3}. All the films cast and dried had an initial porosity on the order of 45–50%. To improve the electrochemical property of the graphite anode, the electrode porosity was controlled at 35% porosity by using a calender machine with a continuously adjustable gap. The electrode laminates were fed through the gap of the calendering machine to compress the

electrode to a desired thickness corresponding to 35% porosity. After being calendered, the electrodes were further dried at 130 °C for 16 h under vacuum before electrochemical studies.

Electrochemical investigation of the electrodes was conducted in standard 2325 coin cells. Lithium foil was used as the counter electrode in the half cells and $Li[Ni_{1/3}Co_{1/3}Mn_{1/3}]O_2$ laminate (from Seimi) containing 10% PVDF and 10% acetylene black was used as the cathode in the full cells. The separator employed was Celgard 2400. The electrolyte from Novolyte was 1 M $LiPF_6$/ethylene carbonate (EC) + diethyl carbonate (DEC) (1:1 by weight ratio). All these cells were tested using a Maccor battery test cycler at 303 K in a Thermotron environmental chamber. Three formation cycles at C/20 were conducted between 0.01 and 1 V versus Li for the half cells and between 3.0 and 4.4 V of the cell voltage for the full cells. Capacity of each cell was determined from the last formation cycle and was used to estimate the C rate for all subsequent cycles. Rate performance test consisted of full discharges at rates of C/10, C/5, C/2, 1C, 2C, 5C, 10C, and 20C, respectively. A charge of C/10 to charge voltage limit preceded each discharge. Long-term cycling test of the graphite/$Li[Ni_{1/3}Co_{1/3}Mn_{1/3}]O_2$ full cells was carried out with 1 C charge to 4.4 V, and followed by 1 C discharge to 3.0 V for 600 cycles. Upon completion of the long-term cycling test, each full cell was dissembled in a glove box at its fully discharged state. Both anode and cathode were harvested and assembled into new half cells to evaluate their electrochemical performance separately.

Morphologies of the fresh and cycled graphite electrodes were imaged by scanning electron microscopy (SEM). The cycled samples were washed with pure dimethyl carbonate (DMC) solvent for several times, dried in vacuum, and then quickly transferred to SEM observation chamber. A JEO FESEM set at 5 kV was used to image the surface of the electrodes.

3. Results and discussion

3.1. Viscosity behavior of the slurries prepared with different mixing technologies

To investigate the interaction between the graphite particles and PVDF binder, dynamic viscosities of the slurries prepared with different mixing technologies were measured at different shear rates. Viscosity variations for these slurries with increasing shear rate are displayed in Fig. 1. As seen in this figure, dynamic viscosity for all the slurries is decreased by increasing shear rate. In the concentrated graphite/AB/PVDF suspensions, the shear thinning is resulted from structural breakdown aroused by increasing shear rate, which is typical non-Newtonian behavior [13]. At each shear rate, dynamic viscosity of the slurries with the same chemical composition shows to be very different according to the mixing technologies. Slurry (I), obtained with a premixed AB/PVDF/NMP mixture, has the lowest viscosity while slurry (II), prepared with a premixed graphite/AB/NMP mixture, shows to be the most viscous. Similar result has been reported for $LiCoO_2$ slurries with different mixing sequences of the slurry components [14]. This phenomenon is believed to be associated with the interaction between the graphite particles and the PVDF binder [15]. For slurry (I), NMP liquid absorption of the active material is very insufficient. This is because the viscosity of the AB/PVDF/NMP mixture is very high compared to pure NMP solvent. As the result, PVDF chain is difficult to stretch into the pores of the active material and there are less free spaces for PVDF in between graphite particles. For slurry (II), free NMP molecules are able to fill the internal region (voids or pores) of the graphite particles before PVDF was added. When PVDF was dissolved into the mixture, the polymer tail can stretch into the pores filled with NMP solvent. Flocculation of the suspension is formed by a bridging process and the slurry shows to be of high viscosity.

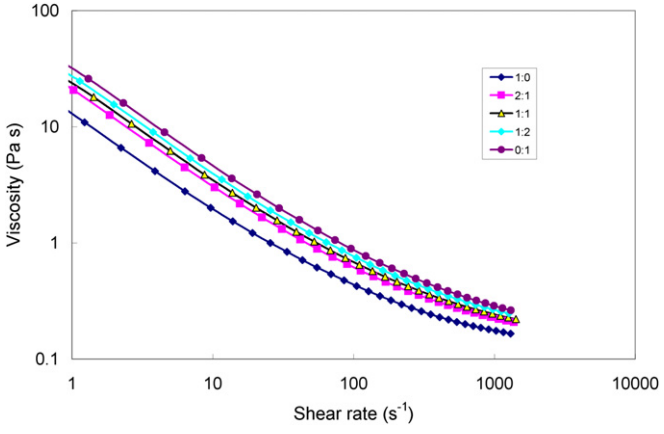

Fig. 1. Dynamic viscosity of the slurries prepared with different mixing technologies at different shear rates.

The viscosity study exhibits that mixing technology induces a deviation in the degree of absorbing liquid for the active material particles. As the result, the configuration of PVDF chain changes from spreading on the active material particle surface to stretching into the voids and pores of the active material particles. This indicates that the physical interaction between graphite and PVDF can be changed by mixing order of the slurry components.

3.2. Physical properties of the graphite laminates prepared with slurries of different mixing technologies

Morphologies of the pristine graphite electrodes at different magnifications are displayed in Fig. 2. From the high magnification images, flat graphitic platelets with distinct edges are observed for the graphite particles. Acetylene black particles are uniformly dispersed on the graphite particle surfaces. Although PVDF binder is not visible within the electrode, from the uniform distribution of the nano-carbon additive, the electrode components are known well dispersed under the experimental condition. By comparison, no obvious morphological difference can be perceived at different magnifications for the graphite laminates prepared with slurries of different mixing technologies.

Fig. 3 compares the electronic conductivity of the graphite laminates measured with a four-point probe technique. Electronic conductivity for all the graphite laminates was obtained to be *ca.* 6.5 S cm^{-1} and the value is not considerably changed by mixing technologies. The conductivity is considerably higher than 1.1 S cm^{-1} of the PVDF/AB film at a ratio of 5:2 (the same ratio as used in this study) as reported by Liu et al. [16,17]. It illustrates that the graphite pellets bear the main role of conducting electrons within the laminate. In this sense, physical disconnection between graphite particles can bring about a significant conductivity loss of the laminate.

Fig. 4a, b displays the breaking stress and Young's modulus of the graphite laminates prepared with slurries of different mixing technologies. Breaking strength is a factor evaluating the adhesion between the graphite particles bound by the PVDF binder. High breaking stress of the laminate is important to avoid the shedding of active materials during battery processing. As it is seen from Fig. 4a, *ca.* 3.7 MPa of the breaking strength was obtained for all the composite laminates. Mixing technology doesn't considerably affect the breaking strength of the graphite laminate.

Young's modulus is a parameter evaluating the elasticity of the composite laminate. The higher the Young's modulus, the greater

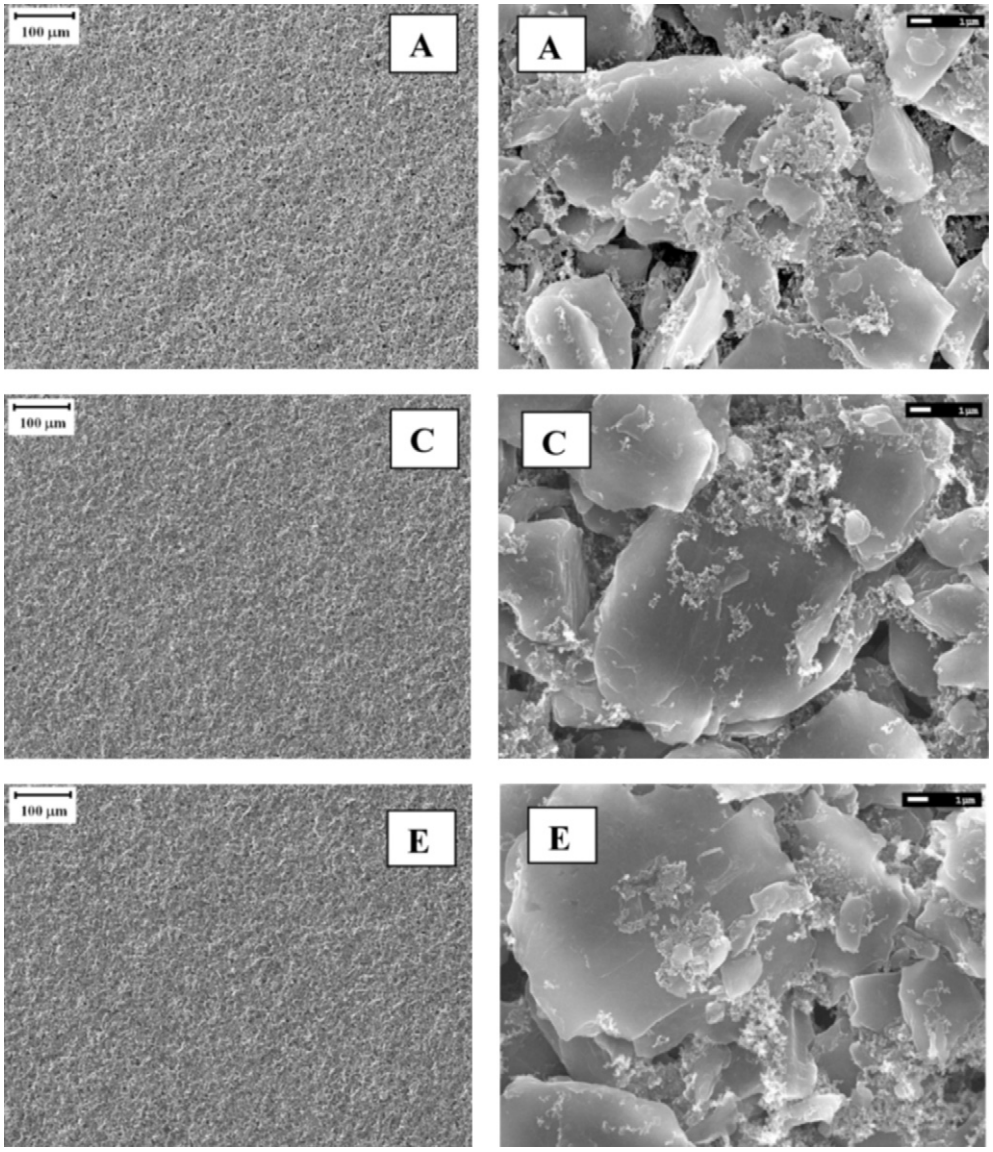

Fig. 2. SEM images of the graphite laminates prepared with slurries of different mixing technologies.

the brittleness of the electrode. It is interesting to see in Fig. 4b that Young's modulus of the graphite laminate is greatly influenced by the mixing technologies of the slurry components. The electrode laminate prepared with slurry (I) has the highest modulus while the modulus of the graphite laminate prepared with slurry (II) is the lowest. The difference in Young's modulus is believed to be associated with the interaction between graphite particles and PVDF binder. As discussed above, for the graphite laminate prepared with slurry (I), it is hard for PVDF chain to stretch into the pores of the graphite particles, most of which only spread onto the graphite surface. There is no much free volume for the PVDF chain in between graphite particles and the laminate shows to be quite brittle. For the graphite laminate prepared with slurry (II), on the other hand, PVDF chain tails can stretch into the pores. PVDF has more free spaces in between graphite particles and the laminate shows to be more flexible. This is consistent with the viscosity behavior of the slurries obtained from rheological studies.

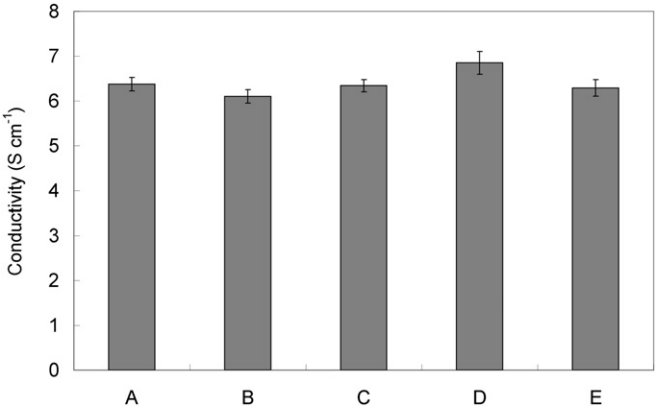

Fig. 3. Electronic conductivities of the graphite laminates prepared with slurries of different mixing technologies.

3.3. Electrochemical properties of the graphite anodes of different mechanics

The first coulombic efficiency, reversible capacity, and rate capability of the graphite anodes prepared with slurries of different mixing technologies were investigated in 1 M $LiPF_6$/EC + DEC(1:1)

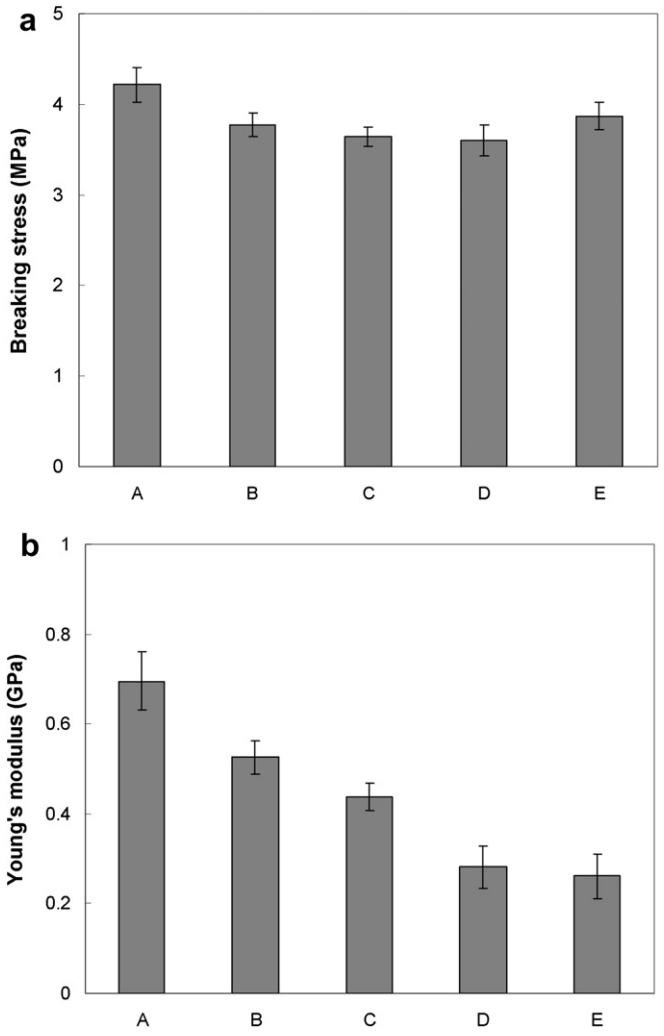

Fig. 4. Breaking stresses (a) and Young's modulus (b) of the graphite laminates prepared with slurries of different mixing technologies.

electrolyte against Li anode. The first coulombic efficiency and reversible capacity were obtained as shown in Fig. 5. Around 93.6% of the first coulombic efficiency and *ca.* 330 mAh g^{-1} of the reversible capacity were obtained for all the five graphite electrodes. No considerable impact of the mechanics is observed on the electrochemical properties in the initial electrochemical cycles.

Rate performance of the graphite anodes prepared with slurries of different mixing technologies was tested and the results are shown in Fig. 6. Rate capability for all the graphite laminates shows to be very identical. In the 0.1–1 C rate range, there is no capacity loss with increasing discharge rate, showing that the electrode capacity is not affected by Li-ion diffusion in this rate regime. A capacity drop-off starts at around 2 C, indicating that 2 C is the maximum current for the graphite anodes to deliver most of its capacity. Further increasing current density induces a dramatic discharge capacity loss. This is because the solid-state diffusion of Li^+ becomes to be the determining factor controlling the rate of the electrochemical reaction. Overall, this result reveals that rate performance of the graphite anode is not related to the mechanical properties of the laminate.

Long-term cycling behavior of the graphite laminates prepared with slurries of different mixing technologies was tested against Li$[Ni_{1/3}Co_{1/3}Mn_{1/3}]O_2$ cathode and the results are shown in Fig. 7. Despite with the same Li$[Ni_{1/3}Co_{1/3}Mn_{1/3}]O_2$ cathode laminate, long-term cycling performances for the full cells displayed a clear distinction. After 600 full capacity charge and discharge cycles, the cells with lower Young's modulus graphite anodes (C, D, and E) retained more than 80% of their initial capacity. Among the less than 20% capacity loss, half of which was consumed in the first 100 cycles and the capacity loss is believed to be ascribed to the SEI rearrangement at the graphite anode surface [18,19]. After 100 cycles, the capacity fade-rate is steady and very identical with each other. For the cells with electrodes (A and B) of higher Young's modulus, similar cycling behavior was observed with those containing lower modulus electrodes in the initial 300 cycles; however, a steep capacity decline occurred after 350 cycles. At the end of the cycling test, the cells with high modulus anodes (A and B) retained only *ca.* 10% of their initial capacity.

In order to identify the failure mechanism for the cells containing high modulus anode, the full cells after long-term cycling test were dissembled in their fully discharged state. Both cathodes and anodes were harvested and new half cells were made with Li anode and fresh electrolyte. Electrochemical behavior of the harvested electrodes was determined and compared with that of the fresh one. Rate capability of the fresh and the cycled Li$[Ni_{1/3}Co_{1/3}Mn_{1/3}]O_2$ cathodes against graphite laminate A and E was plotted in Fig. 8. Compared with the fresh electrode, a small capacity decrease for the cycled Li$[Ni_{1/3}Co_{1/3}Mn_{1/3}]O_2$ cathode at each current density is observed. The capacity decrease is aroused mainly from the dissolution of the active material into electrolyte during the long-term cycling test [20–22]. Rate capability of the

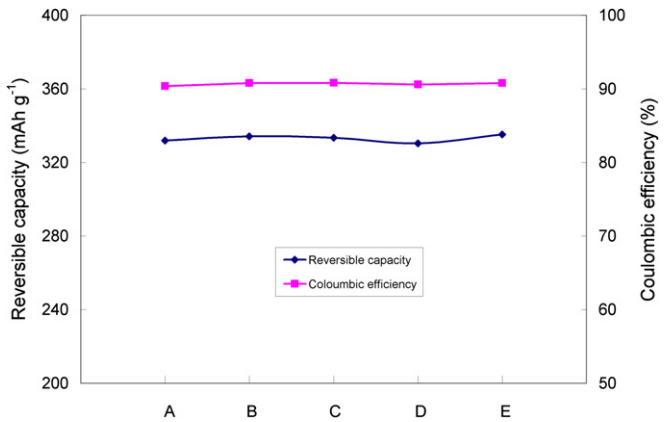

Fig. 5. The first coulombic efficiency and reversible capacity of the graphite electrodes prepared with slurries of different mixing technologies.

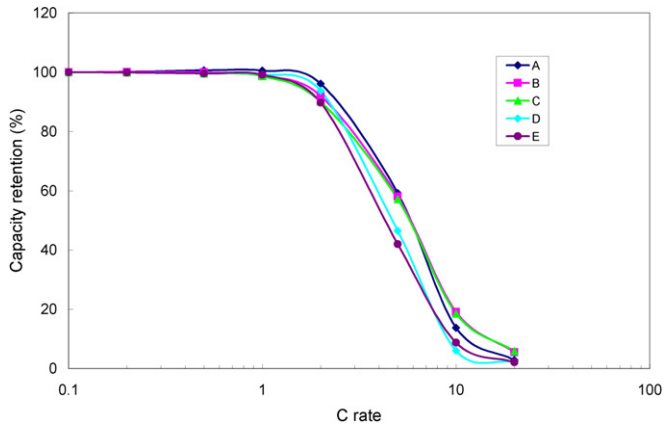

Fig. 6. Rate capability of the graphite anodes prepared with slurries of different mixing technologies.

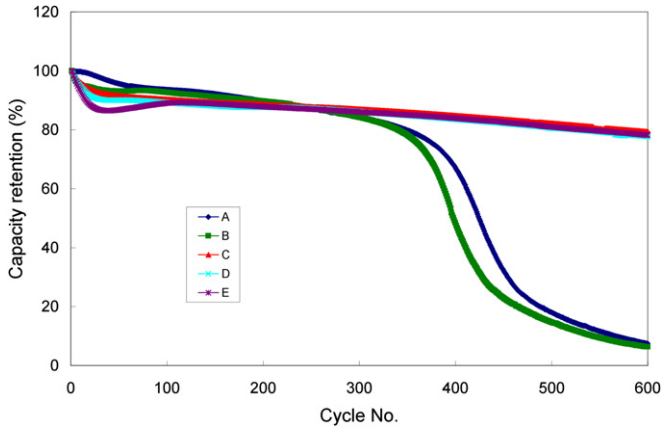

Fig. 7. Long-term cycling performance for the graphite anodes prepared with slurries of different mixing technologies against $Li[Ni_{1/3}Co_{1/3}Mn_{1/3}]O_2$ cathode.

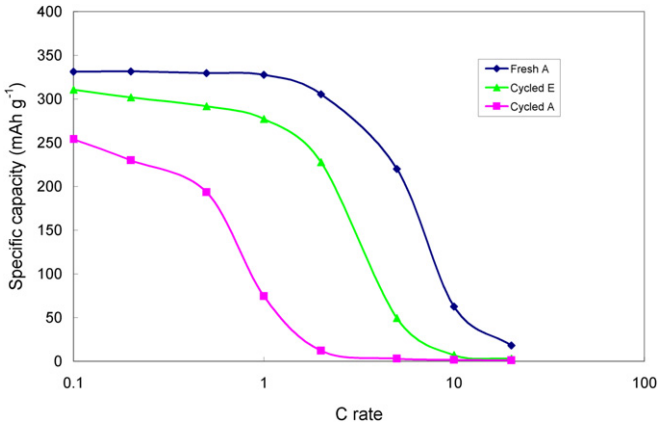

Fig. 9. Rate capability of the fresh graphite anode A and the harvested graphite A and E after long-term cycling test against $Li[Ni_{1/3}Co_{1/3}Mn_{1/3}]O_2$ cathode.

cathodes before and after the cycling test was obtained to be very consistent. A capacity drop at around 2 C shows that the cathode matches well with the fresh anode in rate capability as shown in Fig. 6. The cycled cathodes did not lose much their reversible capacity and rate capability. From this, failure of the full cell with high modulus graphite anode is not originated from the cathode.

Rate capability of the fresh and the harvested CGP-G8 graphite anode A and E is shown in Fig. 9. Compared with the fresh electrode, the harvested graphite anode A lost around 15% of its capacity while the harvested graphite anode E lost 7% of its capacity at C/10 rate. With increasing discharge rate, a steep capacity decline occurred at C/2 for graphite anode A. Considering that the capacity decline starts at 2 C for the fresh electrode, the poor rate performance of graphite anode A after the cycling test reflects a significant resistance increase. At 1 C rate, the same discharge rate with the cycling test of the full cell, graphite anode A lost more than 80% of its initial capacity. This explains the *ca.* 10% capacity retention of the full cell at the end of the cycling test. By contrast, graphite anode E after 600 cycles still retained more than 85% of its initial capacity at 1 C rate. This result reveals that the sharp capacity loss of the full cell containing graphite laminate A is associated with the large rate capability loss. The deterioration of rate performance is believed to be resulted from a large impedance rise of the electrode.

To explain the large resistance rise of the high modulus graphite anode after long-term cycling test, SEM images of the graphite laminate A and E are shown in Fig. 10 at two different magnifications. Many cracks are clearly seen throughout graphite laminate A.

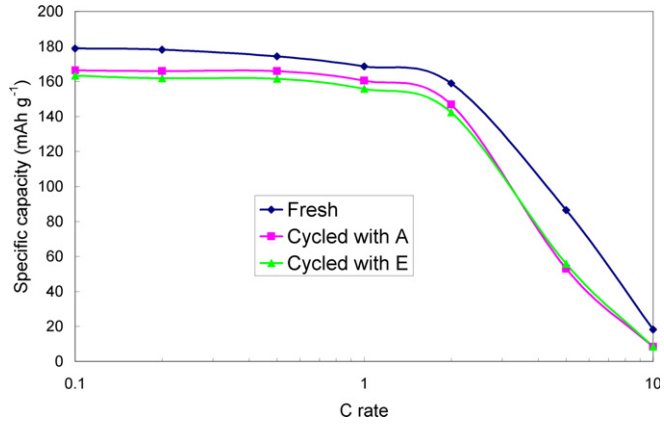

Fig. 8. Rate capability of the $Li[Ni_{1/3}Co_{1/3}Mn_{1/3}]O_2$ cathode before and after long-term cycling test against graphite laminate A and E.

More close examination at higher magnification shows that the crack is formed along the boundaries of the graphite particles. The active material particles did not crack into pieces as they were generally believed. It confirms that the crack of active material particles is less probable to occur compared to the crack of the composite laminate along phase boundaries.

Theoretically, the resistance rise aroused from crack formation and propagation is a slow process. During the long-term cycling test, formation and propagation of cracks and fractures can be described by percolation. At the beginning of the cycling test, few cracks are formed. The connectivity between graphite particles is not damaged at macroscopic scale and the resistance rise of the electrode is negligible. Increasing electrochemical cycle induces more cracks and fractures within the laminate. When the cell undergoes a certain electrochemical cycles (about 350 cycles in this study), percolation of the cracks is developed. Based on percolation theory, there is an exponential growth of the electrode resistance at the critical point where the network of cracks is developed. Correspondingly, we see a sharp capacity decline of the cell between 350 and 450 cycles. Besides the large resistance increase, some active particles may be physically isolated from the electrode laminate and become “dead” active material in the electrode. This explains the relatively high capacity loss at C/10 for the cycled graphite laminate A compared with the graphite E [23–25]. Other reasons including SEI resistance rise and structural failure of the active material is not denied [26,27]; however, considering that the low modulus graphite anode still retained more than 80% of its initial capacity, the main reason for the failure of the high modulus electrode must be associated with the crack formation and propagation within the laminate during electrochemical cycles. In contrast, the mechanical integrity of the low modulus electrode is well maintained after 600 cycles. No obvious crack is observed. Clearly, this result illustrates that there is a close relationship between mechanics and long-term cycling performance for the composite electrode.

3.4. Correlationship between electrode mechanics and long-term cycling performance for the graphite anode

Young’s modulus is an important parameter reflecting the stiffness of the electrode laminate. During Li insertion and extraction process, volume change of active material particles translates into the electrode laminate deformation [28–30]. For an electrode with similar strain, higher stress is generated within the laminate of higher Young’s modulus. Considering the breaking stress of the

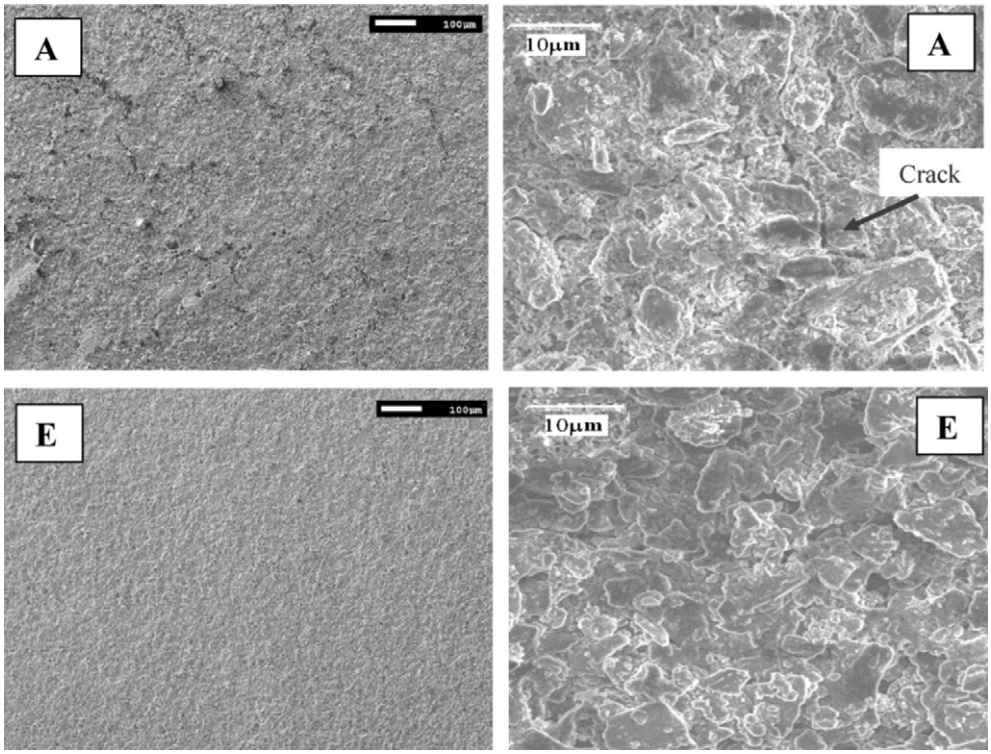

Fig. 10. SEM images of graphite laminate A and E after long-term cycling test against $Li[Ni_{1/3}Co_{1/3}Mn_{1/3}]O_2$ cathode.

graphite laminates prepared with different mixing technologies is very close (around 3.7 MPa), cracks and fatigue fractures are more prone to being induced for the high modulus laminate. As the Young's modulus of the graphite laminates prepared with slurries of different mixing technologies varies from 0.7 to 0.25 GPa (see Fig. 4b), the maximum stain to induce the crack of the electrode laminate is calculated to be from 0.53% to 1.5%. This is significantly lower than the reported *ca.* 10% volume change of graphite particles during lithium intercalation [10,11]. The large discrepancy of the maximum strain between the composite laminate and the graphite particle is believed to come from a couple of sources. One is ascribed to the different test conditions. Electrochemical test was carried out with copper foil while the mechanical properties were determined without copper substrate in this study. Adhesion of the graphite laminate onto copper substrate helps to improve the mechanical properties of the laminate. In this sense, the breaking stress obtained in this study is smaller and the modulus is higher than that of the laminate adhered to copper. The other more important reason is associated with the electrode porosity and low modulus inactive materials. It should be noted that the electrode is porous and 35% porosity exists within the electrode. During Li intercalation, not all the volume change of the particle is translated to the electrode deformation. Some of the volume expansion can be consumed by the voids and pores within the electrode, which has no contribution to the electrode laminate deformation. Besides, the volume growth can also be partially offset by low modulus materials including polymer binder and AB. Taking all these factors into consideration, local strain at the scale of the composite laminate can be an order of magnitude smaller than the strain of the individual graphite crystallite [10].

The results obtained in this study show that mechanical property of the composite laminate plays an important role influencing the long-term cycling performance of the cell. During long-term charge–discharge cycles, crack of the composite laminate is more easily to be induced than the breakage of graphite particles. In this sense, the graphite electrode of low Young's modulus has long durability. In electrode design and fabrication for making lithium ion batteries for EV and PHEV applications, comprehensive understanding and proper optimization of the electrode's mechanical properties are very critical.

4. Conclusion

Mechanical properties of the composite graphite laminate play a subtle and important role affecting the durability of the graphite electrode. A correlation between mechanics and cycling performance for the graphite anode was developed. With the same chemical compositions, Young's modulus of the graphite laminate is very different according to the mixing technology of the slurries. During repeatedly Li insertion and extraction cycles, cracks are easily to be induced within the electrode of high modulus, resulting in physical and electrical disconnection between the active material particles. When the percolation of cracks is developed, an exponential resistance rise leads to a significant rate capability loss of the electrode, which is the main reason responsible for the cell failure.

Large format Li-ion cells for EV applications have an increased likelihood of crack formation and propagation due to their higher energy and power properties. Therefore, design of stable electrode laminates of low Young's modulus and high breaking strength is crucial for the targeted 3000–5000 cycle life. This study shows that Young's modulus of an electrode laminate can be decreased by choosing a proper mixing order of the slurry components. Apart from this, selection of binder of low Young's modulus can be even more effective, which will be subject to further studies.

Acknowledgments

This work was supported by the Assistant Secretary for Energy Efficiency and Renewable Energy, Office of Vehicle Technologies of the U.S. Department of Energy under Contract No. DE-AC02-

05CH11231 and the Natural Science Foundation of China (NSFC 21073129).

References

[1] W. Lu, A. Jansen, D. Dees, P. Nelson, N.R. Veselka, G. Henriksen, J. Power Sources 196 (2011) 1537–1540.
[2] K.M. Kim, W.S. Jeon, I.J. Chung, S.H. Chang, J. Power Sources 83 (1999) 108–113.
[3] H. Zheng, G. Liu, X. Song, P. Ridgway, S. Xun, V.S. Battaglia, J. Electrochem. Soc. 157 (2010) A1060–A1066.
[4] J. Christensen, J. Newman, J. Solid-State Electrochem. 10 (2006) 293–319.
[5] J. Park, W. Lu, A.M. Sastry, J. Electrochem. Soc. 158 (2011) A201–A206.
[6] Y. Hu, X. Zhao, Z. Suo, J. Mater. Res. 25 (2010) 1007–1010.
[7] K. Zhao, M. Pharr, J.J. Vlassak, Z. Suo, J. Appl. Phys. 108 (2010) 073517.
[8] G.G. Botte, Electrochim. Acta 50 (2005) 5647–5658.
[9] S. Renganathan, G. Sikha, S. Santhanagopalan, R.E. White, J. Electrochem. Soc. 157 (2010) A155–A163.
[10] Y. Qi, S.J. Harris, J. Electrochem. Soc. 157 (2010) A741–A747.
[11] R. Reynier, R. Yazami, B. Fultz, J. Power Sources 165 (2007) 616–619.
[12] H. Zheng, R.Z. Yang, G. Liu, X.Y. Song, V.S. Battaglia, J. Phys. Chem. C 116 (2012) 4875–4882.
[13] M. Yoo, C.W. Frank, S. Mori, Chem. Mater. 15 (2003) 850–861.
[14] G. Lee, J.H. Ryu, W. Han, K.H. Ahn, S.M. Oh, J. Power Sources 195 (2010) 6049–6054.
[15] J.-H. Lee, S. Lee, U. Paik, Y.-M. Choi, J. Power Sources 147 (2005) 249–255.
[16] G. Liu, H. Zheng, A.S. Simens, A.M. Minor, X. Song, V.S. Battaglia, J. Electrochem. Soc. 154 (2007) A1129–A1134.
[17] G. Liu, H.H. Zheng, X. Song, V.S. Battaglia, J. Electrochem. Soc. 159 (2012) A214–A221.
[18] M. Dubarry, B.Y. Liaw, J. Power Sources 194 (2009) 541–549.
[19] J. Vetter, P. Novák, M.R. Wagner, C. Veit, K.-C. Möller, J.O. Besenhard, M. Winter, M. Wohlfahrt-Mehrens, C. Vogler, A. Hammouche, J. Power Sources 147 (2005) 269–281.
[20] J. Park, J.H. Seo, G. Plett, W. Lu, A.M. Sastry, Electrochem. Solid-State Lett. 14 (2) (2011) A14–A18.
[21] H.H. Zheng, Q.N. Sun, G. Liu, X.Y. Song, V.S. Battaglia, J. Power Sources 207 (2012) 134–140.
[22] Y. Xia, M. Yoshio, J. Electrochem. Soc. 143 (1996) 825–833.
[23] G. Chen, T.J. Richardson, J. Power Sources 195 (2010) 5387–5390.
[24] G. Kwak, J. Park, J. Lee, S. Kim, I. Jung, J. Power Sources 174 (2007) 484–492.
[25] M. Kerlau, M. Marcinek, R. Kostecki, J. Power Sources 174 (2007) 1046–1051.
[26] D. Zhang, B.S. Haran, A. Durairajan, R.E. White, Y. Podrazhansky, B.N. Popov, J. Power Sources 91 (2000) 122–129.
[27] D.P. Abraham, J.L. Knuth, D.W. Dees, I. Bloom, J.P. Christophersen, J. Power Sources 170 (2007) 465–475.
[28] S. Bhattacharya, A.R. Riahi, A.T. Alpas, J. Power Sources 196 (20) (2011) 8719–8727.
[29] H. Zheng, L. Tan, G. Liu, X. Song, V.S. Battaglia, J. Power Sources 208 (2012) 52–57.
[30] J.P. Owejan, J.J. Gagliardo, S.J. Harris, H. Wang, D.S. Hussey, D.L. Jacobson, Electrochim. Acta 66 (2012) 94–99.